Amplified Spontaneous Emission in Slab Amplifiers

Chana Goren, Yitzhak Tzuk, Gilad Marcus, and Shaul Pearl

***Abstract*—Amplified spontaneous emission (ASE) occurs in media with large gain, and affects both the magnitude and the spatial distribution of the inversion. In this work we theoretically study the effect of ASE in three-dimensional, rectangular slab amplifiers, using Monte Carlo type computer simulations. We found that in one-dimensional amplifiers ASE is always larger at the edges so that the inversion has a maxima at the center of the amplifier. However, in two- and three-dimensional amplifiers, the inversion has a minimum at the center of the amplifier for low gain, and a maximum at the center of the amplifier for high gain. Thus, the inversion profile can be changed by increasing the gain from a minimum at the center, through a plateau, to a maximum at the center. A simple analytical theory was developed and agrees with these results.**

***Index Terms*—Amplified spontaneous emission (ASE), slab amplifiers for high-power lasers.**

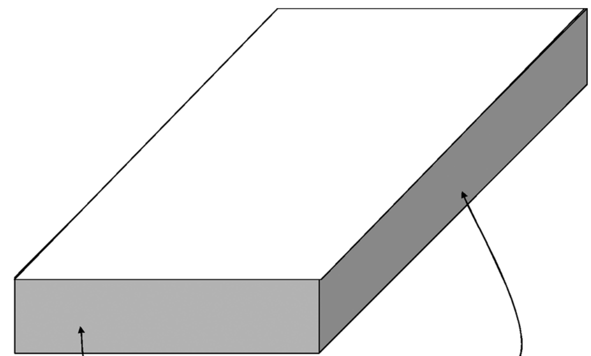

Fig. 1. Rectangular slab amplifier with absorbing edges.

I. Introduction

SPONTANEOUS emission (SE) occurs in any medium with population inversion. This incoherent radiation propagates through the inverted medium and is amplified, though sometimes negligibly. This process is called amplified spontaneous emission (ASE). The larger the gain of the medium, the more the SE is amplified, which results in the reduction of the expected inversion calculated in the absence of ASE. Thus, increasing the gain, results in increased ASE, which decreases the inversion and gain, and leads to limiting of the gain that can be achieved from an amplifier by increasing its size, pumping rate or doping. In addition, the spatial distribution of ASE varies as a function of position in the amplifier, and affects the spatial distribution of the inversion, which results in distortion of the signal. Thus knowledge of the magnitude of ASE and the spatial distribution of the inversion, which is altered by ASE, is useful when planning the dimensions, gain and pumping profile of a laser amplifier.

Most papers discussing ASE, are limited to one-dimensional media such as long laser rods [1], [2], fibers [3], or symmetrically shaped amplifiers [4]. In these systems, for every point in the amplifier one can define a solid angle, into which photons that are emitted have the most significant contribution to ASE. However, in three-dimensional amplifiers of arbitrary shape, this solid angle is very complicated to define, and thus in order to study ASE in these amplifiers, we must numerically calculate the contributions to ASE from all photons spontaneously emitted in this system.

Manuscript received June 11, 2006; revised August 14, 2006.

The authors are with the Non-linear Optics Group, Soreq Nuclear Research Center, Yavne 81800, Israel (e-mail: chana@soreq.gov.il; tzuk@soreq.gov.il; giladm10@yahoo.com; pearl@soreq.gov.il).

Digital Object Identifier 10.1109/JQE.2006.884580

In this work we theoretically study the effect of ASE in three-dimensional, rectangular slab amplifiers, using Monte Carlo type computer simulations. We calculate the gain and pumping efficiency for various amplifiers of different sizes and doping levels, in order to predict the optimum parameters, which will result in the highest efficiency and best spatial distribution of the inversion. In addition, we study the time evolution of the inversion and ASE for both contiunous-wave (CW) pumping and flashlamp pumping.

We examine rectangular amplifiers with edges that are coated with an absorbing substance (cladding) in order to suppress parasitic oscillations (see Fig. 1). In this amplifier, when a photon strikes an edge it is absorbed and when a photon strikes the top or bottom face it either exits the amplifier or is reflected back into the amplifier by TIR (TIR), depending on its angle of incidence with the surface. In addition, a small portion of photons striking the top and bottom faces at angles smaller than the critical angle are reflected back into the system due to Fresnel reflection.

We compare the spatial distribution of the inversion in one-dimensional amplifiers obtained both numerically and analytically, with that obtained numerically in three-dimensional amplifiers. We find both numerically and analytically, that in one-dimensional amplifiers ASE is always larger at the edges of the amplifier, than in the center of the amplifier. Therefore, for one-dimensional amplifiers, the inversion, which is inversely proportional to ASE, has a maxima at the center of the amplifier. However, for three-dimensional amplifiers, the spatial distribution of ASE depends on the gain, and has a maxima in the center for low gain and a minima at the center for high gain. Thus, for three-dimensional amplifiers, the spatial distribution of ASE changes from having a maxima in the

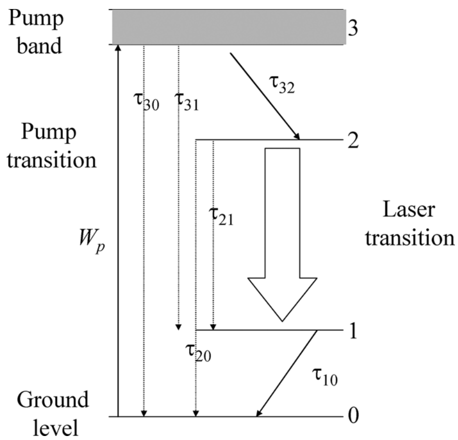

Fig. 2. Energy diagram of a four-level system.

center to a minima in the center as a function of increasing of the gain of the medium.

In addition, we calculate the time evolution of the small-signal gain coefficient, which is linearly proportional to the inversion, for various slab amplifiers, in pulsed flashlamp and CW pumping modes. For pulsed flashlamp pumping we show that in the presence of ASE, maximum inversion is both lower and occurs earlier in the flashlamp pulse, than the maximum inversion in the absence of ASE. For CW pumping, the system reaches a steady state with lower inversion faster than the steady state obtained in the absence ASE. This is due to the limiting nature of ASE in which increasing the inversion results in increased ASE which causes a decrease in the inversion.

II. Rate Equations

We investigated ASE which occurs in a four-level system [5] (see Fig. 2).

Population is pumped from the ground state to the pumping band. We assume that the transition from the pump band to the upper laser level occurs very rapidly, $\tau_{32} \approx 0$, so that the population of the pump band is negligible, i.e. $n_3 \approx 0$. In an ideal four-level system, the terminal laser level, n_1, empties infinitely fast into the ground level, i.e. $\tau_{10} \approx 0$ and $n_1 \approx 0$. In this case the entire population is divided between the ground level zero and the upper level of the laser transition, level 2. We obtain the following rate equations for the ideal four-level system [6]:

$$\frac{dn}{dt} = -c\sigma n\phi - \frac{n}{\tau} + W_p(n_{\text{tot}} - n) \tag{1}$$

$$\frac{d\phi}{dt} = c\sigma n\phi + \frac{n}{\tau^*} - c\frac{d\phi}{ds} \tag{2}$$

where n is the density of the inverted population, W_p is the pumping rate, n_{tot} is the total density of the active population, σ is the stimulated emission cross section, τ is the life time of the excited state, ϕ is the flux, s is the path of the flux in the amplifier, d/ds is the directional derivative along path s and τ^* is the lifetime of the photons traveling along the path s.

In the absence of external flux, the flux, ϕ, which appears in (1) and (2), originates in spontaneously emitted photons, which propagate through the amplifier and are amplified by the inverted population in the amplifier.

III. Computer Simulation

We calculate the effect of ASE on the population inversion in a three-dimensional amplifier by numerically solving the rate equations for each point in a three-dimensional amplifier.

$$\begin{aligned} n_{i+1}(x,y,z) = n_i(x,y,z) + \Big(&-\sigma n_i(x,y,z)c\phi(x,y,z) \\ &- \frac{n_i(x,y,z)}{\tau} + W_p\left(n_{\text{tot}} - n_i(x,y,z)\right)\Big)\Delta t \end{aligned} \tag{3}$$

where n is the density of the inverted population, ϕ is the flux, which is due to the propagating spontaneously emitted photons, W_p is the pumping rate, n_{tot} is the density of the Nd^{3+} ions, σ is the absorption cross section, and τ is the life time of the excited state.

Before the pump is turned on, there is no stored energy in the amplifier and the population inversion equals zero, $n_0(x,y,z) = 0$. When the pumping is turned on, population is excited to the upper laser level, n, which in turn, starts to spontaneously decay. The number of ions excited into the upper energy level, for each unit volume during a small time interval, $\Delta \mathrm{t}$ is given by

$$W_p\Delta t\left(n_{\text{tot}} - n_i(x,y,z)\right)dxdydz. \tag{4}$$

The number of ions that decay from the excited energy level per unit volume, during the time interval is equal to

$$\frac{n_i(x,y,z)}{\tau}\Delta t dxdydz. \tag{5}$$

This includes both radiative and nonradiatively decays from the excited state. The nonradiative losses are affected both by intrinsic processes that depend on the glass structure during manufacturing, such as multi photon relaxation, cross relaxation and excitation migration, as well as extrinsic processes that depend on impurities in the glass laser (e.g., OH and transition metal ions) [6]. Thus the value of τ depends on the concentration of the Nd^{3+} ions and changes with the change of the Nd^{3+} concentrations. The number of photons which are spontaneously emitted from each unit volume is

$$\phi_0(x,y,z) = \frac{n_i(x,y,z)}{\tau}\Delta t dxdydz\eta_{\text{FE}} \tag{6}$$

where η_{FE} is the fluorescence efficiency which is the fraction of ions in the excited state that decay by emitting a photon. These photons are emitted in many wavelengths, whose branching ratios β and emission cross sections σ depend on the properties of the amplifier [7], [8]. We calculate the flux, ϕ, of the propagating photons for each wavelength, along their path of propagation in the gain medium

$$\begin{aligned} &(c\phi(x+ds_x, y+ds_y, z+ds_z)) \\ &\quad = (c\phi(x,y,z))\exp\Big[\sigma n_i(x,y,z)\left(c\phi(x,y,z)\right) \\ &\qquad \times\sqrt{ds_x^2 + ds_y^2 + ds_z^2}\Big]. \end{aligned} \tag{7}$$

IV. Gain

The gain of an amplifier is given by [6]

$$G = e^{\sigma n l} \tag{8}$$

where σ is the stimulated emission cross section, n is the population inversion in the medium and l is the distance that the photons traveled in the medium. It is convenient to define the small-signal gain coefficient [6], which defines the gain of the amplifier per unit length

$$g_0 = \sigma n. \tag{9}$$

V. Pumping

There are two methods for pumping the amplifier, continuously using a diode, or by flashlamps. The pumping rate, which appears in the rate equations ((1), (2)), is related to the pumping power P before bleaching, by

$$W_p = \frac{P}{h\nu n_{\text{tot}} L_x L_y L_z} \tag{10}$$

where P is the pumping power, ν is the laser frequency, n_{tot} is the total population, and L_x, L_y, and L_z are the dimensions of the amplifier.

A. Pumping by Flashlamps

The flashlamp power profile is given by [9]

$$P = 4\eta \frac{E_L}{t_f} \left(\frac{t}{t_f}\right)^2 e^{-\frac{2t}{t_f}} \tag{11}$$

where E_L is the pumping energy, t_f is the time of the maximum of the pulse, and η is the conversion efficiency of electrical energy to photons. t_f is related to the pulsewidth $\Delta T_{1/3}$ which is given at $(1/3)P_{\max}$, by

$$\Delta T_{\frac{1}{3}} = 2.161 t_f. \tag{12}$$

Fig. 3 shows a typical flashlamp pumping profile (dotted curve) calculated from (11), and the resulting small-signal gain (solid curve) in the absence of ASE which is calculated from (1) by setting $\phi = 0$. We see that the small-signal gain continues increasing past the maximum of the flashlamp power, and reaches its maximum value sometime after the maximum power of the flashlamp.

B. CW Pumping

When the amplifier is pumped continuously, the system reaches a steady state. In the absence of ASE we calculate the small-signal gain coefficient analytically by setting $\phi = 0$ and $(dn/dt) = 0$ in (1). We get the asymptotical small-signal gain at $t \to \infty$

$$g_0 = \frac{W_p n_{\text{tot}} \sigma}{\frac{1}{\tau} + W_p} \underset{W_p \ll \frac{1}{\tau}}{\longrightarrow} W_p n_{\text{tot}} \sigma \tau. \tag{13}$$

We plot the time evolution of the inversion in the absence of ASE, by numerically solving (1) when $\phi = 0$ (see Fig. 4).

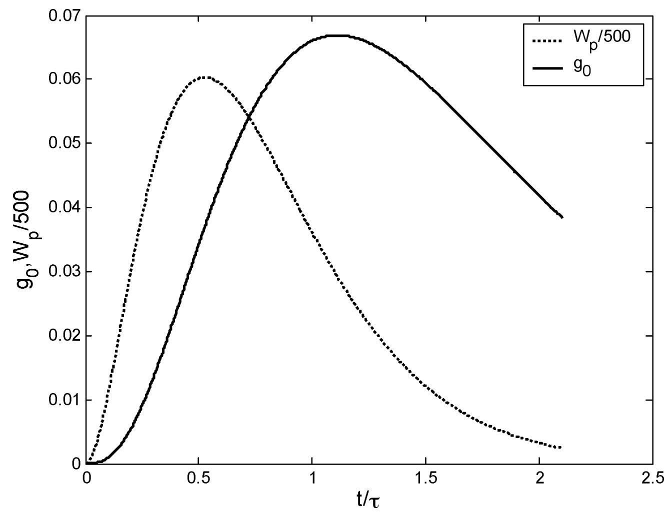

Fig. 3. Numerical calculation of g_0 and of the flashlamp pumping profile, in the absence of ASE.

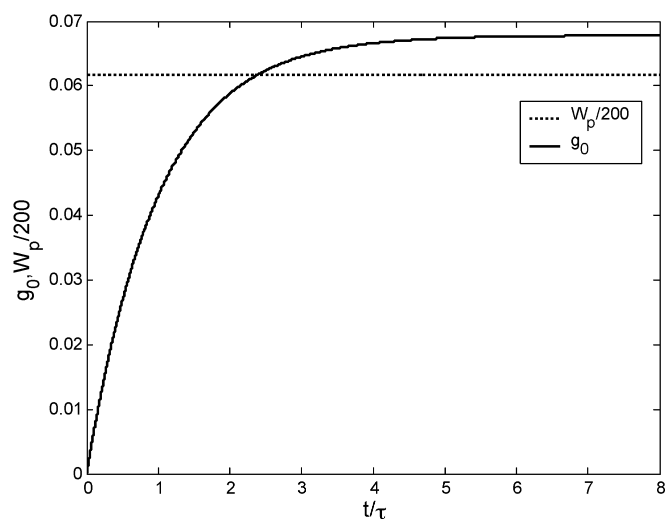

Fig. 4. Numerical calculation of g_0, for a CW pumped system, in the absence of ASE.

VI. Nd:Glass

The energy levels and some fluorescence lines of Nd^{3+} are shown in Fig. 5.

The emission spectra of Nd:Glass consists of three large bands which are attributed to the $^4F_{3/2} \rightarrow ^4 I_{9/2}$, $^4I_{11/2}$ and $^4I_{13/2}$ transitions. The exact wavelengths, branching ratios and lifetimes of these transitions, depend on the glass used [11]. Here we use the values of the branching ratios and lifetimes obtained by Ajroud *et al.* [10] and multiply the cross sections by a constant so the cross section at the 1053 nm is equal to $4.2{\cdot}10^{-20}$ cm^2. In Figs. 6 and 7 we plot the SE wavelength and cross section distributions. In this case the fluorescence is centered at 896, 1053, and 1324, with branching ratios $\beta = 0.3$, 0.59, 0.11, stimulated emission cross sections $\sigma = 1.48 \cdot 10^{-20}$ cm^2, $4.2 \cdot 10^{-20}$ cm^2 and $2.016 \cdot 10^{-20}$ cm^2, respectively, with a line width of $\Delta\lambda = 29.3$ nm.

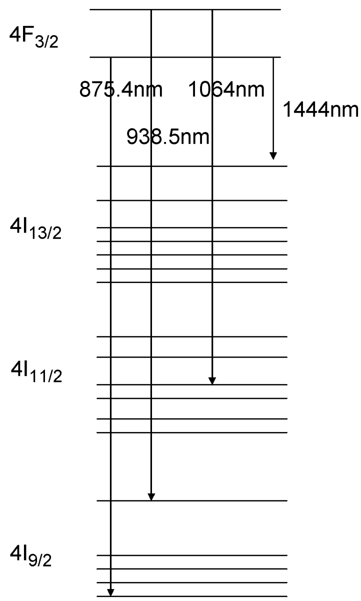

Fig. 5. Energy levels of Nd^{3+}.

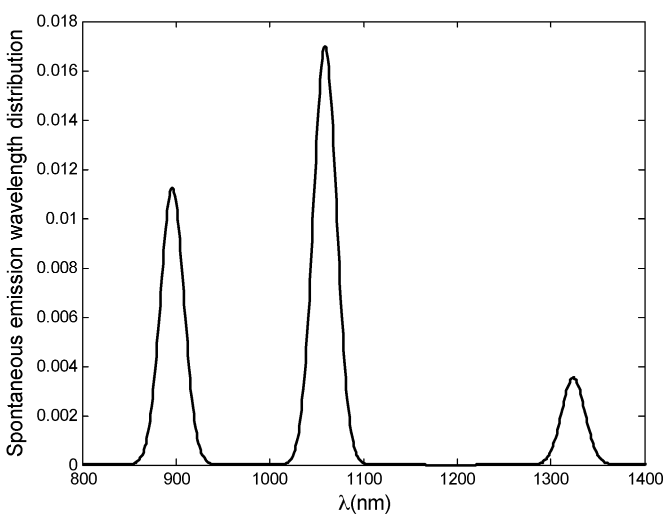

Fig. 6. Wavelength distribution of the SE for an arbitrary Nd:glass sample.

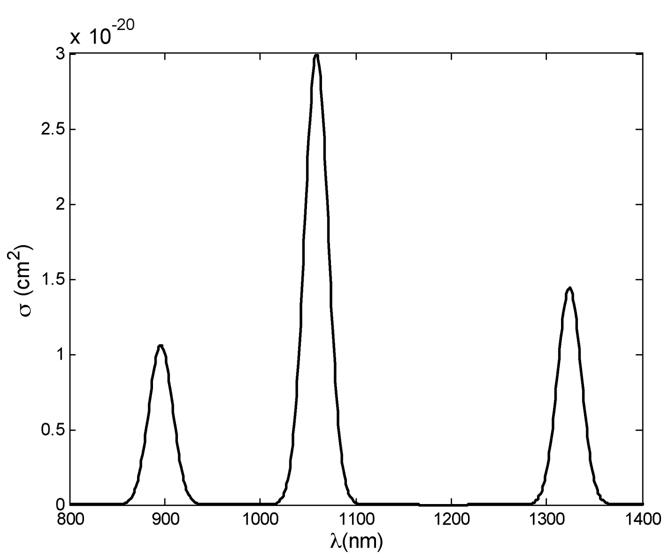

Fig. 7. σ distribution as a function of the SE wavelengths.

A. Pumping Efficiency in Nd:Glass

Typically, the PFN electrical efficiency is 70%–90% of the bank energy to the flashlamps, with the remainder lost as heat in the circuit elements [11]. Flashlamp plasmas convert about 80% of the delivered electrical energy to photons, with approximately half the output energy falling in the 400–1000-nm region of the Nd^{3+} pumping bands, which is the energy needed in our case. Usually the UV light (<400 nm) is deliberately absorbed in the lamp glass by using cerium doped glass, in order to protect the laser material from solarization. As these photons circulate in the pump cavity, some are reabsorbed by the flashlamp plasma, a fraction of which are reemitted, some are absorbed by the metal reflectors or slab holders and some are lost through the ends of the amplifiers. The remaining photons, about 10% of those emitted by the plasma are absorbed by the laser slabs. Photons absorbed by the laser slabs, produce stored energy in the form of excited Nd^{3+} ions.

B. Fluorescence Efficiency in Nd:Glass

Fluorescence efficiency $\eta_{\rm FE}$ is the fraction of photons pumped into the upper level which decay by emitting photons. Fluorescence efficiency is never unity, due to nonradiative losses which are affected by intrinsic processes that depend on the glass structure during manufacturing, such as multi phonon relaxation, cross relaxation and excitation migration, as well as extrinsic processes that depend on impurities in the glass laser (e.g., OH and transition metal ions) [9]. The value of fluorescence efficiency ranges from 0.5 [12] to 0.9 [13] depending on the Nd^{3+} concentration, the exact composition of the glass as well as the care with which the glass was manufactured.

C. Monte Carlo Simulations

We wrote a number of Monte Carlo type computer codes which calculate the inverted population evolution and the flux due to SE, both for CW and flashlamp pumping. We wrote a standard Monte Carlo simulation in which, in each time interval, five random numbers determine the position (x, y, z) and direction (φ, θ) of the spontaneously emitted beam. The spectral distribution of these photons is determined by the specific amplifier medium.

The trajectory of this beam is calculated, assuming that the edges of the amplifier are totally absorbing (Fig. 1). When the beam reaches one of the two non absorbing faces it is reflected back into the amplifier if $\theta > \theta_c = \sin^{-1}(1/n)$ TIR angle, where n is the index of refraction of the amplifier. If $\theta < \theta_c$ the photon exits the amplifier, neglecting the Fersnel fraction which is reflected back into the amplifier. The next beam of photons, emitted from a new random site in a random direction, sees lower inversion where the first beam traveled. In Fig. 8, we show some random trajectories of photons in the amplifier.

In addition, we wrote more deterministic and faster programs, in which we calculate the amplification of the SE from each point, assuming that it is not affected by other points emitting during the specified time interval. For these programs, we need only two random numbers to determine the direction (φ, θ) of the photons emitted from each point.

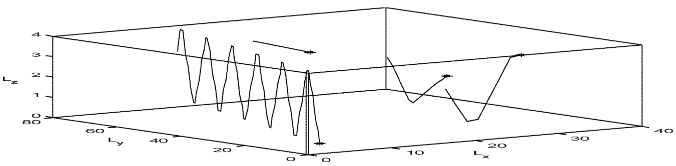

Fig. 8. Examples of random trajectories inside an amplifier with absorbing edges.

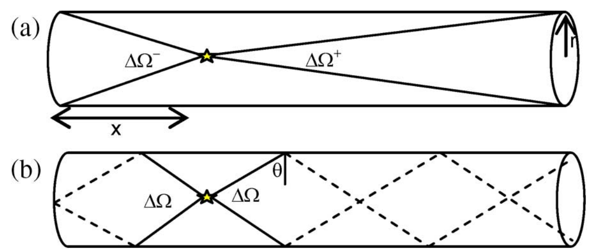

Fig. 9. (a) Photons striking the edge of the amplifier are absorbed. (b) Photons striking the edge of the detector are reflected if $\theta > \theta_c$ and exit the system if $\theta < \theta_c$.

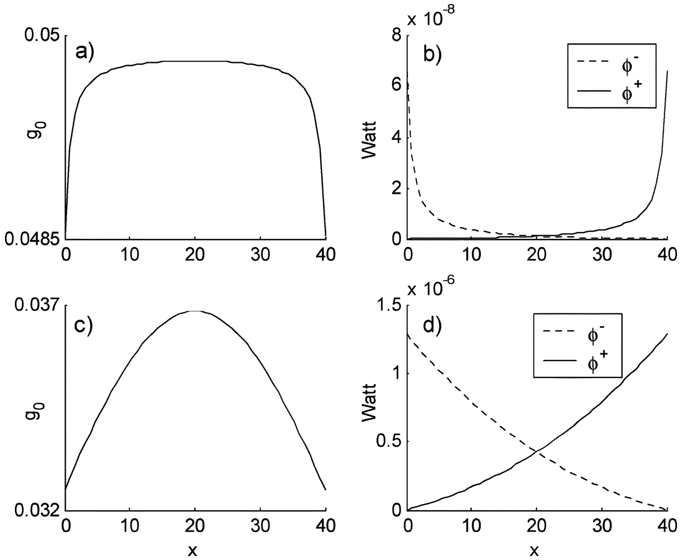

Fig. 10. Calculated g_0 for a 40-cm-long amplifier (a) for the case of geometrical angle and and (b) for the case of (c) TIR and (d) $\sigma = 4.2 \cdot 10^{-20}$ cm^2, $\tau = 300\ \mu$s, $n_{\rm tot} = 4.2 \cdot 10^{20}$ cm^{-3}, $n = 1.528$ and $W_p = 16.4265\ s^{-1}$, which in the absence of ASE results in $g_0 = 0.05$ cm^{-1}.

VII. Results

A. One-Dimensional Amplifiers

In one-dimensional amplifiers, photons can propagate either in the positive or in the negative directions [2], [3]. The rate equations [(1), (2)] for this case are written as

$$\frac{dn}{dt} = -c\sigma n(\phi^+ + \phi^-) - \frac{n}{\tau} + W_p(n_{\rm tot} - n) \quad (14)$$

$$\frac{d\phi^+}{dt} = c\sigma n\phi^+ + \frac{n}{\tau^*} - c\frac{d\phi^+}{dx} \quad (15)$$

$$\frac{d\phi^-}{dt} = c\sigma n\phi^- + \frac{n}{\tau^*} + c\frac{d\phi^-}{dx} \quad (16)$$

where ϕ^+ and ϕ^- are photons propagating in the positive and negative directions, respectively.

For long amplifiers, the contribution to ASE of the spontaneously emitted photons that propagate to the end of the amplifier is much larger than that of the photons which strike the edge. Thus the inversion in these amplifiers can be calculated by using (14)–(16) for one-dimensional amplifiers, while taking into account in (15) and (16) only the photons that reach the edge of the amplifier. At each point, photons are spontaneously emitted in all directions. The solid angle $\Delta\Omega$, defines the angle into which photons are emitted, and reach the end of the amplifier. Two geometries for $\Delta\Omega$ are plotted in Fig. 9.

In Fig. 9(a), photons striking the edge of the amplifier are absorbed so that $\Delta\Omega = \int_0^{2\pi} d\varphi \int_0^{\Omega} \sin\theta d\theta$, is the solid geometrical angle on the exit plane defined in (17) and (18)

$$\Delta\Omega^+ = 2\pi\left(1 - \frac{L-x}{\sqrt{(L-x)^2 + r^2}}\right) \quad (17)$$

$$\Delta\Omega^- = 2\pi\left(1 - \frac{x}{\sqrt{x^2 + r^2}}\right). \quad (18)$$

In Fig. 9(b), the photons are reflected if the angle of incidence is larger than the critical angle. In this case all photons emitted in an angle larger than θ_c, undergo TIR and reach the edge of the amplifier. The solid angle into which photons are emitted and reach the end of the amplifier is given by

$$\Delta\Omega = 2\pi\left(1 - \frac{1}{n}\right) \quad (19)$$

and $1/\tau^*$ is related to $\Delta\Omega$ by

$$\frac{1}{\tau^*} = \frac{\Delta\Omega}{4\pi\tau}. \quad (20)$$

We solve (14)–(16) in the steady state by setting $(dn/dt) = 0$ and $(d\phi^\pm/dt) = 0$. The boundary conditions of these coupled partial differential equations are that the number of photons propagating in the positive direction at $x = 0$, is equal to zero, and the number of photons at $x = \mathrm{L}$ propagating in the negative direction, is also equal to zero. We plot the solution of (14)–(16) for a 40 cm long Nd:glass rod, with all other parameters taken from [6]. In Fig. 10(a) and (b), we plot g_0 and the flux due to ASE for the rod with the absorbing edge [see Fig. 9(a)] and in Fig. 10(c) and (d), we plot g_0 and the flux due to ASE for the same rod with TIR [see Fig. 9(b)].

In comparing Fig. 10(b) and (d), we see that the effect of ASE is larger for a rod with TIR. This is due to a larger average $\Delta\Omega$ for the case of TIR, than $\Delta\Omega$ obtained by the geometrical angle. Larger ASE results in lower g_0 as can be seen by comparing g_0 for both cases edge [see Fig. 10(a) and (c)].

In order to check out our three-dimensional MonteCarlo program we calculate ASE in a one-dimensional amplifier by setting θ, which is the angle between $\hat{z}$ and the point where the photon is emitted to $\pi/2$, and using one random number to determine if $\varphi = 0$ or π, i.e. if the photon is propagating in the positive or negative direction. We find that the numerical calculations are identical to the analytical results.

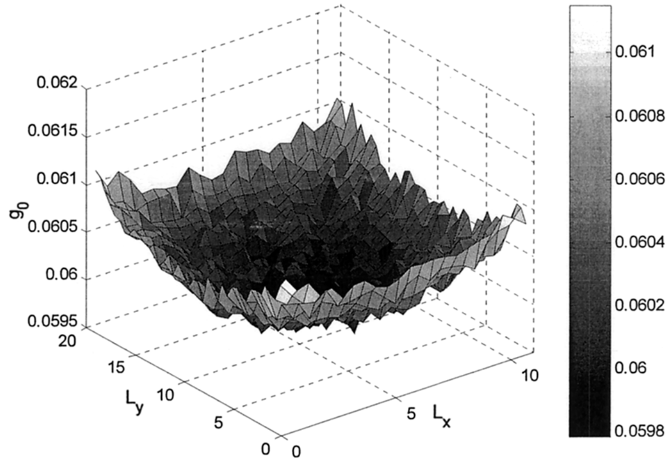

Fig. 11. Small-signal gain coefficient in the steady state. $L_x = 11$ cm, $L_y = 20$ cm, $L_z = 2.4$ cm $W_p = 14.1185\ s^{-1}$, which results in $g_0 = 0.062\ \text{cm}^{-1}$ in the absence of ASE. $\sigma = 4.2 \cdot 10^{-20}$ cm^2, $\tau = 300\ \mu$s, $n_{\text{tot}} = 4.2 \cdot 1020$ cm^{-3}, $\eta_{\text{FE}} = 0.8$.

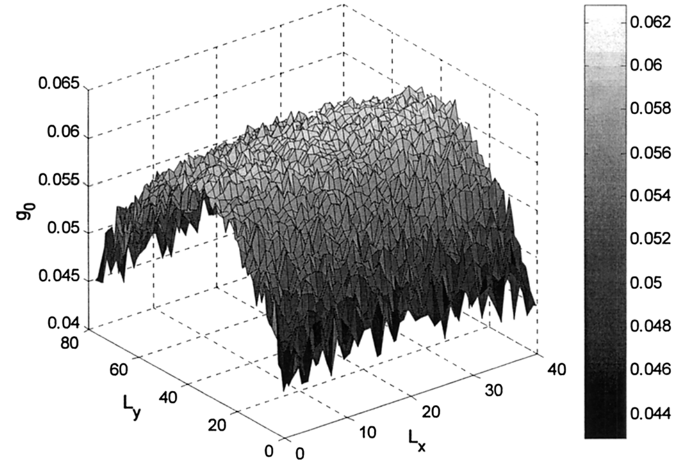

Fig. 12. Small-signal gain coefficient in the steady state $L_x = 40$, $L_y = 80$, $L_z = 4$, $W_p = 11.7158\ s^{-1}$, which results in $g_0 = 0.062\ \text{cm}^{-1}$ in the absence of ASE. $\sigma = 4.2 \cdot 10^{-20}$ cm^2, $\tau = 300\ \mu$s, $n_{\text{tot}} = 4.2 \cdot 10^{20}$ cm^{-3}, $\eta_{\text{FE}} = 0.8$.

B. Two- and Three-Dimensional Amplifiers

In a two-dimensional amplifier, photons are emitted in a plane at a random angle φ and are amplified until they reach an absorbing edge. We calculate ASE in a two-dimensional amplifier by using our three-dimensional simulation and setting θ, which is the angle between $\hat{z}$ and the point where the photon is emitted to $\pi/2$.

In the three-dimensional amplifier, photons reaching the faces of the amplifier are either totally reflected back into the amplifier or exit the system (neglecting Fresnel reflection), depending on their angle. Those reflected back into the amplifier are absorbed when they reach the edges.

We find that the small-signal gain distribution is similar for two and three-dimensional slabs. In calculating the inversion and small-signal gain we use the SE and stimulated emission cross section plotted, respectively, in Figs. 6 and 7.

We plot the small-signal gain coefficient in the steady state for two slabs of different sizes, which have identical small-signal gain coefficients in the absence of ASE. When ASE is taken into account in the calculation we found that for a small slab, g_0 has a minima in the center (Fig. 11), whereas for a larger slab, g_0 has a maxima in the center (Fig. 12).

In contrast to the one-dimensional case where the inversion and small-signal gain coefficient, are always higher in the center of the amplifier, for two and three-dimensional amplifiers the spatial distribution of the inversion changes from a minima in the center to a maxima in the center as a function of the amplifier gain.

C. Time Evolution of the Inversion

We plot the time evolution of g_0, for a large slab pumped by flashlamp pumping (Figs. 13 and 14) and by CW pumping (Figs. 15 and 16). In Fig. 13, we plot the time evolution of g_0 in the case of flashlamp pumping in the presence and absence (brown curve) of ASE. We compare the time evolution of g_0 in the absence of ASE with g_0 in the presence of ASE at various points in the slab. We calculate the well known result, that maximum g_0 occurs some time after the peak of the flashlamp power. In addition, we show that maximum g_0 in the presence of ASE is reached before the maximum in the absence of ASE. This is expected from the limiting nature of ASE. Increasing the inversion, increases the gain, this results in increasing ASE, which lowers the gain.

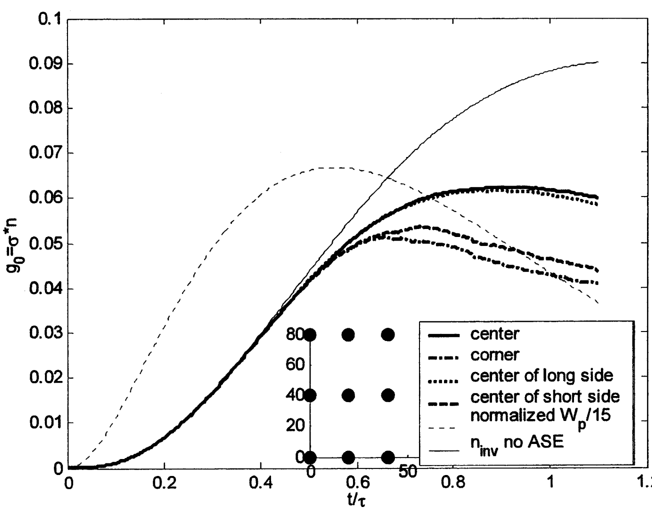

Fig. 13. Time evolution of the small-signal gain coefficient at different points in a large amplifier. $L_x = 40$ cm, $L_y = 80$ cm, $L_z = 4$ cm, $n_{\text{tot}} = 3.5\ 10^{20}$ cm^{-3}, $\sigma = 4.2\ 10^{-20}$ cm^2, $\tau = 300\ \mu$s. The SE and cross section distributions are given in Figs. 6 and 7.

In Fig. 14, we plot the inversion profile of the amplifier after 0.3τ, 0.5τ, 0.9τ, and τ, where τ is the excited state life time. When the gain is small, g_0 is lower in the center of the amplifier Fig. 14(a). As the inversion increases, the longer dimenesion, which has higher gain develops higher inversion in the center whereas the short dimension, whose gain is not high enough for developping higher g_0 in the center, has higher gain at the edge Fig. 14(b). At maximum inversion both dimensions have lower inversion at the edges than in the center Fig. 14(c).

In Fig. 15, we plot the time evolution of g_0 for the same slab amplifier, for CW pumping. We choose $W_p = 19.7966\ s^{-1}$ which results in $g_0 = 0.0911\ \text{cm}^{-1}$ in the absence of ASE, which

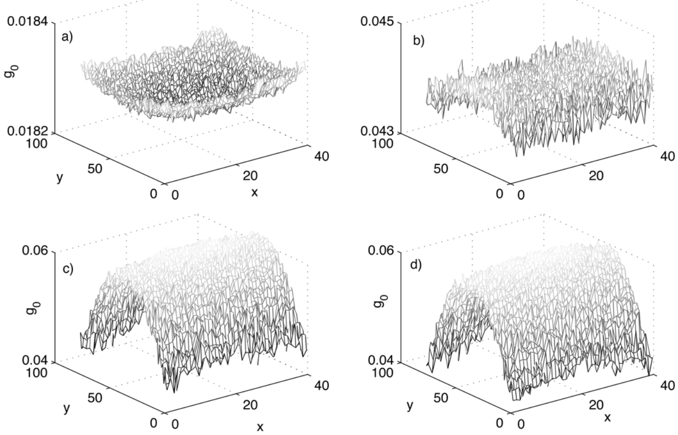

Fig. 14. Small-signal gain coefficient after (a) 0.3τ, (b) 0.5τ, (c) 0.9τ, and (d) τ. All other parameters are the same as Fig. 13.

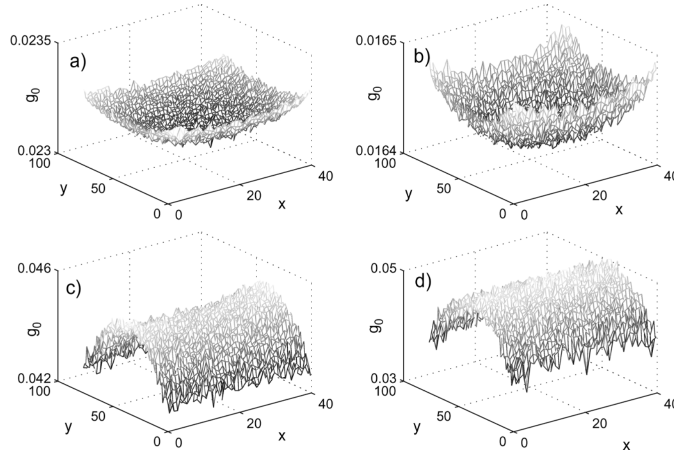

Fig. 16. Small-signal gain coefficient after (a) 0.3τ, (b) 0.5τ, (c) 0.9τ, and (d) 8τ. All other parameters are the same as Fig. 13. $W_p = 19.79\ s^{-1}$ we use the same parameters as in Fig. 13.

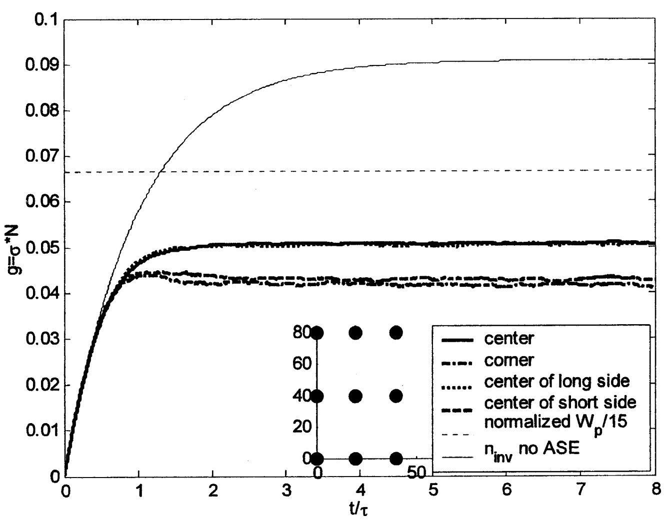

Fig. 15. Time evolution of g_0 at different points in the amplifier, for the CW pumping scheme. Amplifier parameters are the same as in Fig. 13.

is the maximum value of g_0 obtained by flashlamp pumping in the absence of ASE. We show that in the presence of ASE, g_0 reaches the steady state before it would have reached there in the absence of ASE emphasizing the limiting nature of ASE.

In Fig. 16, we plot the small-signal gain profile after 0.3τ, 0.5τ, 0.9τ, and τ in the large slab. We see that when the gain is small, g_0 is lower in the center [Fig. 16(a) and (b)]. As the inversion increases, the longer dimension, which has higher gain, has higher g_0 in the center whereas the shorter dimension, which has lower gain, has higher g_0 at the edge of the amplifier Fig. 16(c). At maximum inversion both axis have lower inversion at the edges Fig. 16(d).

D. Scaling

One can change the dimensions and the small-signal gain coefficient g_0, of an amplifier, while keeping the gain $e^{g_0 l}$ which is calculated neglecting the effects of ASE, constant. As expected, the gain calculated when taking ASE into account, is identical for both amplifiers.

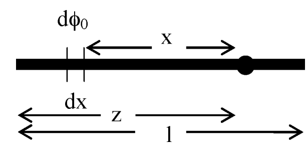

Fig. 17. One-dimensional amplifier of length l.

VIII. Analytical Calculation

We calculated simplified analytical expressions, for the flux due to ASE, in the steady state for one and two-dimensional slabs. This flux is inversely proportional to the population inversion. We compare these simplified expressions, with the results obtained by the numerical simulation.

A. One-Dimensional Amplifier

We start with an amplifier of length l, which at $t = 0$ has a constant photon density, ϕ_0 (see Fig. 17).

The flux resulting from a unit length is

$$d\phi_0 = \frac{\phi_0 dx}{l}. \tag{21}$$

This flux is emitted in the $\pm$ directions. Therefore, the flux due to this element, at a distance x is amplified, and equals

$$d\phi = \frac{1}{2} d\phi_0 e^{g_0 x} = \frac{\phi_0}{2l} e^{g_0 x} dx. \tag{22}$$

At any point z in the amplifier, the total flux is a sum of the flux resulting from all elements of the amplifier

$$\phi(z) = \int_0^z d\phi + \int_0^{l-z} d\phi = \frac{\phi_0}{2 g_0 l}\left(e^{g_0 z} + e^{g_0 (l-z)} - 2\right). \tag{23}$$

This function has a minimum at $z = 1/2$ for any g_0 and l. Thus, for one-dimensional amplifiers, the inversion and small-signal gain coefficient, which are proportional to $1/\phi$ [see (1)],

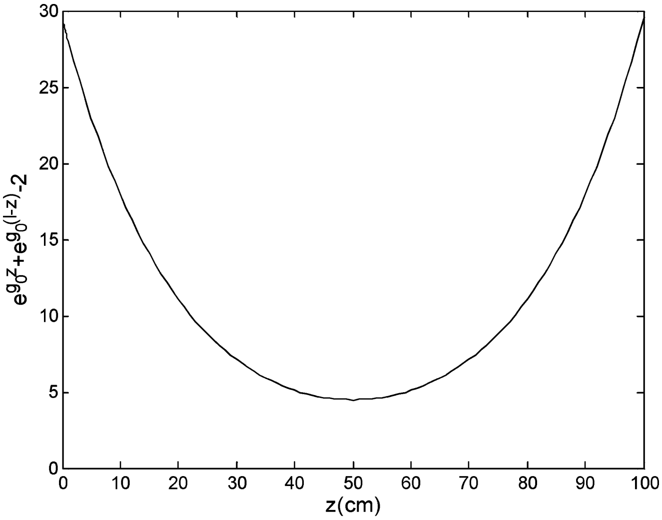

Fig. 18. $(e^{g_0 z} + e^{g_0(l-z)} - 2)$, which is proportional to the flux for a one-dimensional rod, $l = 100$ cm, $g_0 = 0.05$ cm^{-1}.

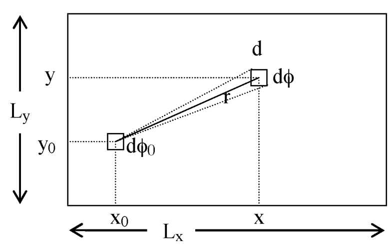

Fig. 19. Two-dimensional amplifier.

all have a maximum at $z = (1/2)$. In Fig. 18, we plot $(e^{g_0 z} + e^{g_0(l-z)} - 2)$ in a rod with $l = 100$ cm, $g_0 = 0.05$ cm^{-1}.

B. Two-Dimensional Amplifier

We calculate the flux at each point of a two-dimensional amplifier, which at $\mathrm{t} = 0$ has a constant photon density of ϕ_0 (see Fig. 19)

The flux resulting from a unit area is

$$d\phi_0 = \frac{\phi_0 dxdy}{L_x L_y}. \tag{24}$$

The flux is emitted in all directions. Therefore, the angle η, into which photons that are emitted at (x_0, y_0), reach (x, y) is

$$\eta = \frac{\sqrt{2}d}{2\pi r}. \tag{25}$$

The flux at a distance r from this element is

$$d\phi = \eta d\phi_0 e^{g_0 r}. \tag{26}$$

The flux at a point (x, y) in the amplifier results from all the elements in the two-dimensional slab

$$\phi(x,y) = \frac{\phi_0 d}{\sqrt{2}\pi L_x L_y} \int_0^{L_y}\int_0^{L_x} \frac{1}{\sqrt{(x-x_0)^2+(y-y_0)^2}} \times \exp\left(g_0\sqrt{(x-x_0)^2+(y-y_0)^2}\right) dxdy. \tag{27}$$

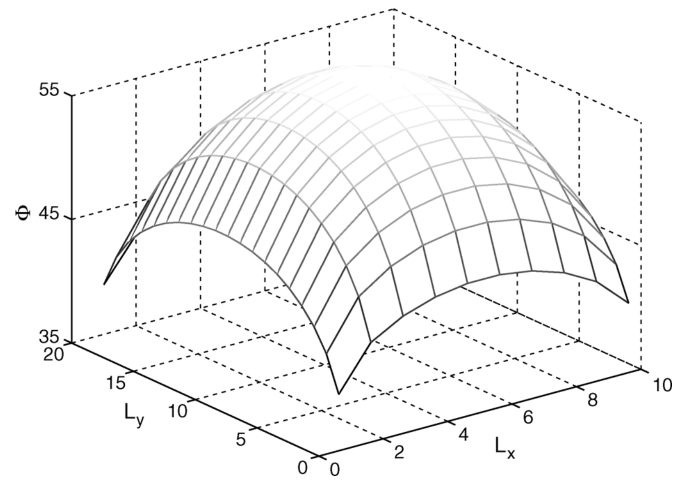

Fig. 20. Φ for a slab with low gain is higher in the center than at the edge, $L_x = 10$ cm, $L_y = 20$ cm, $g_0 = 0.05$ cm^{-1}.

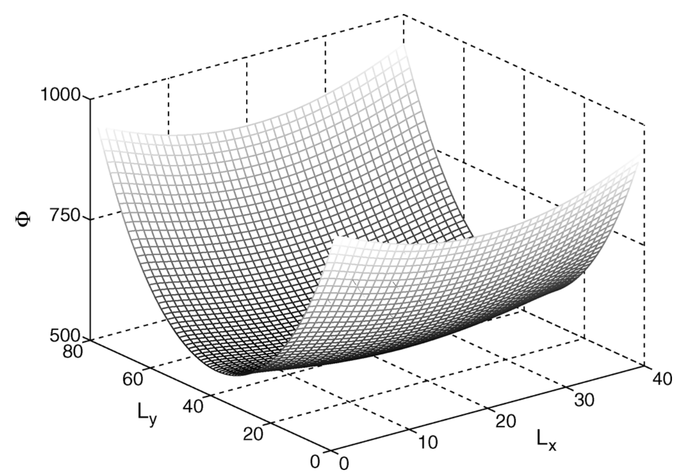

Fig. 21. Φ for a slab with high gain is lower in the center than at the edge, $L_x = 40$ cm, $L_y = 80$ cm, $g_0 = 0.05$ cm^{-1}.

In Figs. 20 and 21, we plot

$$\Phi = \int_0^{L_y}\int_0^{L_x} \frac{1}{\sqrt{(x-x_0)^2+(y-y_0)^2}} \times \exp\left(g_0\sqrt{(x-x_0)^2+(y-y_0)^2}\right) dxdy$$

which is inversely proportional to the inversion and small-signal gain coefficient.

We see that for slabs with low gain (Fig. 20) the flux is higher at the center of the slab, which results in g_0 being lower in the center as we obtained by our numerical simulation (Fig. 11). When the gain is high (Fig. 21) the flux is lower in the center, resulting in higher inversion and small-signal gain coefficient in the center of the slab, which is the result that we obtained in our numerical simulation (Fig. 12).

IX. Conclusion

We investigated the phenomena of ASE in laser amplifiers. We calculated ASE in rod and slab amplifiers, both numerically and analytically. We showed that for one-dimensional amplifiers ASE is always larger at the edges, resulting in higher inversion at the center of the amplifier. However, this is not the case for two and three-dimensional amplifiers. For these amplifiers when the gain is low, the inversion is lower at the center of the amplifier and for higher gain, the inversion is higher at the center.

REFERENCES

[1] L. Allen and G. I. Peters, "Amplified spontaneous emission and external signal amplification in an inverted medium," *Phys. Rev. A*, vol. 8, pp. 2031–2047, 1973.

[2] P. A. Schultz, K. F. Wall, and R. L. Aggarwal, "Simple model for amplified spontaneous emission in a Ti : Al_2O_3 amplifier," *Opt. Lett.*, vol. 13, pp. 1081–1083, 1988.

[3] C. R. Giles and E. Desurvire, "Modeling Erbium-doped fiber amplifiers," *J. Lightw. Technol.*, vol. 19, no. 2, pp. 271–282, Feb. 1991.

[4] J. B. Trenholme, Fluorescence amplification and parasitic oscillation limitations in disc lasers Naval Research Lab., Washington, D.C., NRL Memorandum, Report No. 2480, 1972.

[5] W. Koechner, *Solid State Laser Engineering*. New York: Springer-Verlag, 1999.

[6] J. H. Campbell, Recent advances in phosphate laser glasses for high power applications Lawrence Livermore Nat. Lab., Univ. Califonia, Livermore, Rep. No. 2317000, 1996.

[7] D. W. Hall and W. J. Weber, "Modeling gain saturation in neodymium laser glasses," *IEEE J. Quantum Electron.*, vol. QE-20, no. 8, pp. 831–834, Aug. 1984.

[8] Y. C. Ratnakaram, R. P. S. Chakradhar, K. P. Ramesh, J. L. Rao, and J. Ramakrishna, "The effect of host glass on optical absorption and fluorescence of Nd^{3+} in $x\mathrm{Na_2O} - (30 - x)\mathrm{K_2O} - 70\mathrm{B_2O_3}$ glasses," *J. Phys.: Condens. Matter*, vol. 15, pp. 6715–6730, 2003.

[9] Y. Tzuk, Feb. 2006, private communication.

[10] M. Ajroud, M. Haouari, H. Ben Ouada, H. Maaref, A. Brenier, and C. Garapon, "Investigation of the spectroscopic properties of Nd^{3+}-doped phosphate glasses," *J. Phys.: Condens. Matter*, vol. 12, pp. 3181–3193, 2000.

[11] A. C. Erlandson, M. D. Rotter, D. N. Frank, and R. W. McCracken, Design and Performance of the Beamlet Amplifiers ICF Quarterly Report, Oct.-Dec. 1996, UCRL-LR-105821-95-1.

[12] J. G. Edwards, "Measurement of the cross-section for stimulated emission in neodymium-doped glass from the output of a free running laser oscillator," *J. Phys. D.*, vol. 1, pp. 449–456, 1968.

[13] A. J. Ramponi and J. A. Caird, "Fluorescence quantum efficiency and optical heating efficiency in laser crystals and glasses by laser calorimetry," *J. App. Phys.*, vol. 63, pp. 5476–5484, 1988.

Chana Goren received the Ph.D. degree in physics from Bar Ilan University, Ramat Gan, Israel, in 2004. Her thesis research focused on nonlinear high-resolution laser spectroscopy of atoms.

Since 2005, she has been with the Soreq Nuclear Research Center, Yavne, Israel, as a Physicist in the Nonlinear Optics Group.

Yitzhak Tzuk received the Ph.D. degree in physics from Ben-Gurion University of the Negev, Beer Sheva, Israel, in 1992. His thesis research focused on dynamics of the detonation products of primary explosives.

From 1993 to 1994, he was with the El-Op Company as a physicist in the lasers division in research and development. Since 1994, he has been with the Soreq Nuclear Research Center, Yavne, Israel, as a Senior Physicist in the Nonlinear Optics Group.

Gilad Marcus received the Ph.D. degree in physics from Hebrew University, Jerusalem, Israel, in 2005.

Since 2005 he has been with the Soreq Nuclear Research Center, Yavne, Israel, as a physicist in the Nonlinear Optics Group.

Shaul Pearl received the Ph.D. degree in physics from Ben-Gurion University of the Negev, Beer Sheva, Israel, in 2005.

Since 1999 he has been with the Soreq Nuclear Research Center, Yavne, Israel, as a physicist in the Nonlinear Optics Group.